*Original Scientific Paper*

# Position-Parameter Selection Criterion for a Helix-Curve Meshing-Wheel Mechanism Based on Sliding Rates

Jiang Ding – Yangzhi Chen* – Yueling Lv – Changhui Song

South China University of Technology, China

*The space curve meshing wheel (SCMW) is an innovative gear mechanism mediating transmission between space curves instead of classic space surfaces; the most common type of SCMW is the helix curve meshing wheel (HCMW). In this study, we propose a position-parameter selection criterion of the HCMW based on its slide rates. The sliding rates of the contact curves at the meshing point are defined and calculated; the optimal meshing condition of the HCMW is attained by analyzing the features of the slide rates; the position-parameter selection criterion is subsequently attained as well as corresponding contact curve equations. Both simulation and practical examples using different position-parameters are provided to verify the transmission continuity, and their slide rates are calculated. The calculating result shows that the HCMW coincident with the position-parameter selection criterion has better slide rates and, therefore, can have better tribological performance. The design method proposed in this paper aims to change the current situation so that the position-parameters of the HCMW are determined according to designers' experience, and theoretically provides a foundation for its standardized production in industry.*
*Keywords: gear, space curve meshing wheel, helix curve meshing wheel, position-parameter, parameter selection, sliding rate*

## 0 INTRODUCTION

Closely related to the friction and wear performances of meshing gear teeth, the slide rate is an important index for estimating the transmission quality of a gear pair [1]. To reduce wear and to prevent the scuffing of the gears, the slide rates of the two surfaces should be close and minimized in many situations. For example, in precision instruments, cycloid gears with the same slide rates at every meshing point are more commonly used than involute gears, which have different slide rates at different meshing points. As the traditional gear pairs mediate transmission between two conjugate surfaces [2] to [4], the current research is mainly about the slide rates between two surfaces [5] and [6].

Recently, the Space Curve Meshing Wheel (SCMW) was proposed, based on the space curve meshing theory [7] to [10], instead of the classic space surface meshing theory [2]. Mediating transmission between the contact curves on the surfaces of the driving and driven tines, the SCMW possessed the advantages of small size, a large transmission ratio, and high design flexibility.

Since its invention, progress has been attained in many aspects, including meshing equations [7] to [11], design criteria [12], contact ratio [13], bending stress [14], manufacturing technology [15] and [16], and practical application [17] to [21]. At present, the most common SCMW is the Helix Curve Meshing Wheel (HCMW), as shown in Fig. 1.

The modification coefficients of the transitional gears are important factors affecting the slide rates of the conjugate surfaces; similarly, the position-parameters ($a$ and $b$ in Fig. 1, further details in section 1.2) of the HCMW influence the meshing radii and, subsequently, the slide rates of the contact curves. However, the position-parameters are currently selected according to designers' experience. If they are not selected properly, the slide rates may be so large that the tines will wear out quickly.
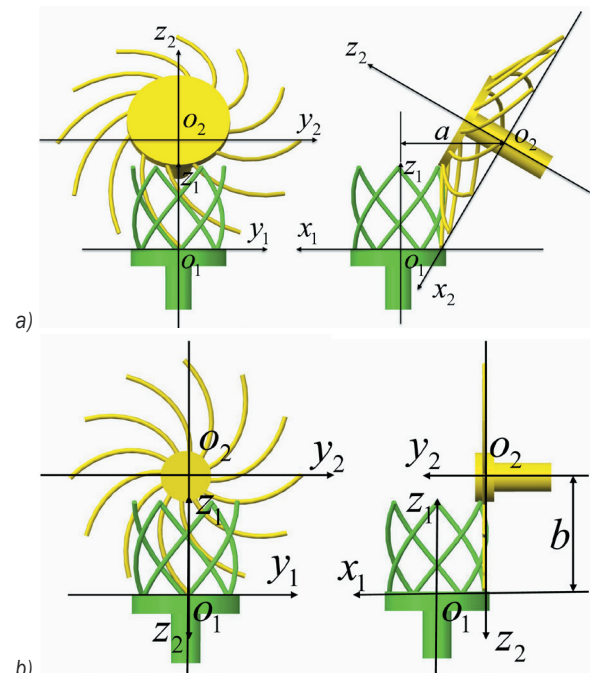


**Fig. 1.** *Helix Curve Meshing Wheel; a) non-vertical case and b) vertical case*

In this paper, a position-parameter selection criterion for the HCMW based on its slide rates

---

*Corr. Author's Address: South China University of Technology, School of Mechanical and Automotive Engineering, Guangzhou, China, meyzchen@scut.edu.cn

is proposed. It should be noted that the position-parameters also affect other parameters, such as the maximum radius or the height of the HCMW pair, but their effects on the meshing radii and the subsequent slide rates are direct and primary. Additionally, the space curve meshing skew gear mechanism (SCMSGM) in [11] is the latest SCMW. However, its geometric conditions remain under research, and its slide rates will be studied afterward.

According to its current application [17] to [21], this study mainly focuses on the HCMW under operation conditions of self-lubrication and dry friction. In addition, the relative slide speed between the driving and driven tines should be preserved to form a hydrodynamic film with lubricant to reduce the wear under operation conditions. The definitions of the slide rates are still available in that occasion, while the position-parameter selection criterion is slightly different.

# 1 SLIDE RATES

## 1.1 Slide Rates between Two Conjugate Space Curves

The working part of the SCMW is a pair of conjugate space curves named "contact curves". As shown in Fig. 2, suppose that the contact curves, which are denoted as $\Gamma_1 : r_1 = r_1^{(1)}(t)$ and $\Gamma_2 : r_2 = r_2^{(2)}(t)$, mesh at point $M$ at the given start moment. After a period of $\Delta t$, point $M_1$ on the curve $\Gamma_1$ meshes with point $M_2$ on the curve $\Gamma_2$. The corresponding arc lengths are denoted as $\widehat{MM_1} = s_1$ and $\widehat{MM_2} = s_2$, while the corresponding chord lengths are $|\overrightarrow{MM_1}| = |\Delta r_1|$ and $|\overrightarrow{MM_2}| = |\Delta r_2|$. Therefore, $\lim\limits_{\Delta t \to 0} s_1 = \lim\limits_{\Delta t \to 0} |\Delta r_1|$ and $\lim\limits_{\Delta t \to 0} s_2 = \lim\limits_{\Delta t \to 0} |\Delta r_2|$.
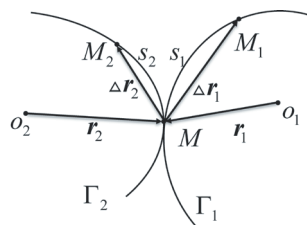
**Fig. 2.** *Slide rates of conjugate space curves*

The slide rates of space curves are defined as the limit value of the ratio of the lengths difference between two relative arcs divided by the length of the given arc:

$$\sigma_1 = \lim_{s_1 \to 0} \frac{s_1 - s_2}{s_1} = \lim_{\Delta t \to 0} \frac{|\Delta r_1| - |\Delta r_2|}{|\Delta r_1|}, \qquad (1)$$

$$\sigma_2 = \lim_{s_2 \to 0} \frac{s_2 - s_1}{s_2} = \lim_{\Delta t \to 0} \frac{|\Delta r^{(2)}| - |\Delta r^{(1)}|}{|\Delta r^{(2)}|}. \qquad (2)$$

The slide directions of $\Gamma_1$ and $\Gamma_2$ can be attained from either Eqs. (1) or (2). Take Eq. (1) for example: when $\sigma_1 > 0$, i.e. $s_1 > s_2$, the relative slide direction of $\Gamma_2$ comparing with $\Gamma_1$ is from $M$ to $M_2$ and consistent with the moving direction of the meshing point; when $\sigma_1 < 0$, i.e., $s_1 < s_2$, the relative slide direction of $\Gamma_2$ comparing with $\Gamma_1$ is from $M_2$ to $M$ and reverse with the moving direction of the meshing point.

## 1.2 Slide Rates of the SCMW Contact Curves

As the SCMW is mainly designed to operate in conditions with low loads, the elastic deformation [12] has insignificant impact on the slide rates, and the contact curve equations of the SCMW are used for analysis.

The contact curve equations are attained in the space curve meshing coordinates, as shown in Fig. 1. The coordinate $o_1 - x_1 y_1 z_1$ is stationary with respect to the driving wheel, and the coordinate $o_2 - x_2 y_2 z_2$ to the driven wheel. In a non-vertical case, the distance from $o_2$ to $x_1$ is denoted as $a$; in a vertical case, the distance from $o_2$ to $z_1$ as $b$.

As shown in Fig. 2, the driving and driven contact curves of the SCMW are denoted as $r_1^{(1)} = \begin{bmatrix} x_M^{(1)} & y_M^{(1)} & z_M^{(1)} \end{bmatrix}^T$ in $o_1 - x_1 y_1 z_1$ and $r_2^{(2)} = \begin{bmatrix} x_M^{(2)} & y_M^{(2)} & z_M^{(2)} \end{bmatrix}^T$ in $o_2 - x_2 y_2 z_2$. Their differential equations are as in Eqs. (3) and (4):

$$\frac{d_1 r_1^{(1)}}{dt} = \begin{bmatrix} x'^{(1)}_M & y'^{(1)}_M & z'^{(1)}_M \end{bmatrix}^T, \qquad (3)$$

$$\frac{d_2 r_2^{(2)}}{dt} = \begin{bmatrix} x'^{(2)}_M & y'^{(2)}_M & z'^{(2)}_M \end{bmatrix}^T, \qquad (4)$$

$$\lim_{\Delta t \to 0} \frac{|\Delta r_1|}{|\Delta r_2|} = \left| \frac{d_1 r_1^{(1)}}{dt} \right| \bigg/ \left| \frac{d_2 r_2^{(2)}}{dt} \right| = \frac{|d_1 r_1^{(1)}|}{|d_2 r_2^{(2)}|}. \qquad (5)$$

From Eqs. (1) and (3) to (5), the slide rate of the driving contact curve is as in Eq. (6):

$$\sigma_1 = 1 - \frac{\sqrt{\left(x'^{(2)}_M\right)^2 + \left(y'^{(2)}_M\right)^2 + \left(z'^{(2)}_M\right)^2}}{\sqrt{\left(x'^{(1)}_M\right)^2 + \left(y'^{(1)}_M\right)^2 + \left(z'^{(1)}_M\right)^2}}. \qquad (6)$$

From Eqs. (2) to (5), the slide rate of the driven contact curve is as in Eq. (7):

$$\sigma_2 = 1 - \frac{\sqrt{\left(x'^{(1)}_M\right)^2 + \left(y'^{(1)}_M\right)^2 + \left(z'^{(1)}_M\right)^2}}{\sqrt{\left(x'^{(2)}_M\right)^2 + \left(y'^{(2)}_M\right)^2 + \left(z'^{(2)}_M\right)^2}}. \qquad (7)$$

## 1.3 Slide Rates of the HCMW Contact Curves

The driving contact curve of the HCMW in $o_1-x_1y_1z_1$ is circular helix curve, and its equation is as below [9]:

$$\begin{cases} x^{(1)}_M = m_1 \cos t \\ y^{(1)}_M = m_1 \sin t \ (t_S \le t \le t_E), \\ z^{(1)}_M = n\pi + nt \end{cases} \qquad (8)$$

where $m_1$ is the helix radius, $m_1 > 0$; $n$ is the pitch coefficient, equaling the ratio of the pitch and $2\pi$ [9], and usually $n > 0$ as the driving cylindrical helix is a right-hand screw; $t$ is an independent parameter indicating the length of the contact curve; $t_s$ and $t_E$ are the starting and ending values for the meshing point, respectively.

In this paper, $t_s = -\pi$, so the initial value of the driving contact curve height is $z^{(1)}_M = 0$, which means that the driving curve begins from the plane $x_1o_1y_1$; $t_E = -\pi/2$, i.e., $t_E - t_s = \pi/2$, so a quarter of a circle is used.

The transmission ratio of the HCMW pair is denoted as $i_{12}$, and the angle between the angular velocity of the driving and driven wheels is denoted as $\theta$, $0 \le \theta \le \pi$. The driven contact curves for non-vertical and vertical cases are reflected in Eqs. (9) and (10), respectively [9]:

$$\begin{cases} x^{(2)}_M = \left(\dfrac{m_1 - a}{\cos\theta} - n(t+\pi)\sin\theta\right)\cos\dfrac{t+\pi}{i_{12}} \\ y^{(2)}_M = -\left(\dfrac{m_1 - a}{\cos\theta} - n(t+\pi)\sin\theta\right)\sin\dfrac{t+\pi}{i_{12}}, \\ z^{(2)}_M = -n(t+\pi)\cos\theta \end{cases} \qquad (9)$$

$$\begin{cases} x^{(2)}_M = -(nt+n\pi-b)\cos\dfrac{t+\pi}{i_{12}} \\ y^{(2)}_M = (nt+n\pi-b)\sin\dfrac{t+\pi}{i_{12}} \\ z^{(2)}_M = 0 \end{cases} \qquad (10)$$

Eqs. (9) and (10) are a common conical helical curve and a planar Archimedean helical curve,

respectively. It can be proved from both Eqs. (9) and (10) that the initial value of the driven contact curve height is $z^{(2)}_M = 0$, and the driven curve begins from the plane $x_2o_2y_2$.

Differential equations of Eqs. (8) to (10) are as in Eqs. (11) to (13):

$$\begin{cases} x'^{(1)}_M = -m_1 \sin t \\ y'^{(1)}_M = m_1 \cos t \ , \\ z'^{(1)}_M = n \end{cases} \qquad (11)$$

$$\begin{cases} x'^{(2)}_M = -\dfrac{1}{i_{12}}\left(\dfrac{m_1-a}{\cos\theta} - n(t+\pi)\sin\theta\right)\sin\left(\dfrac{t+\pi}{i_{12}}\right) + \\ \qquad + n\sin\theta\cos\left(\dfrac{t+\pi}{i_{12}}\right) \\ y'^{(2)}_M = -\dfrac{1}{i_{12}}\left(\dfrac{m_1-a}{\cos\theta} - n(t+\pi)\sin\theta\right)\cos\left(\dfrac{t+\pi}{i_{12}}\right) -, \\ \qquad -n\sin\theta\sin\left(\dfrac{t+\pi}{i_{12}}\right) \\ z'^{(2)}_M = -n\cos\theta \end{cases} \qquad (12)$$

$$\begin{cases} x'^{(2)}_M = \dfrac{nt+n\pi-b}{i_{12}}\sin\dfrac{t+\pi}{i_{12}} - n\cos\dfrac{t+\pi}{i_{12}} \\ y'^{(2)}_M = \dfrac{nt+n\pi-b}{i_{12}}\cos\dfrac{t+\pi}{i_{12}} + n\sin\dfrac{t+\pi}{i_{12}}. \\ z'^{(2)}_M = 0 \end{cases} \qquad (13)$$

From Eqs. (6), (11) and (12), the slide rates of the HCMW contact curve for non-vertical case are as in Eqs. (14) and (15):

$$\sigma_1 = 1 - \frac{\sqrt{\left[\dfrac{1}{i_{12}}\left(\dfrac{m_1-a}{\cos\theta} - n(t+\pi)\sin\theta\right)\right]^2 + n^2}}{\sqrt{m_1^2 + n^2}}, \qquad (14)$$

$$\sigma_2 = 1 - \frac{\sqrt{m_1^2 + n^2}}{\sqrt{\left[\dfrac{1}{i_{12}}\left(\dfrac{m_1-a}{\cos\theta} - n(t+\pi)\sin\theta\right)\right]^2 + n^2}}. \qquad (15)$$

From Eqs. (7), (11) and (13), the slide rates of the HCMW contact curve for vertical case are as in Eqs. (16) and (17):

$$\sigma_1 = 1 - \frac{\sqrt{\left(\dfrac{nt + n\pi - b}{i_{12}}\right)^2 + n^2}}{\sqrt{m_1^2 + n^2}}, \qquad (16)$$

$$\sigma_2 = 1 - \frac{\sqrt{m_1^2 + n^2}}{\sqrt{\left(\dfrac{nt + n\pi - b}{i_{12}}\right)^2 + n^2}}. \qquad (17)$$

## 2 POSITION-PARAMETER SELECTION CRITERION BASED ON SLIDE RATE

### 2.1 Monotonicity and Feasible Region of Sliding Rates

The non-vertical HCMW is illustrated as an example. Differentials of Eqs. (14) and (15) are as in Eqs. (18) and (19), respectively:

$$\sigma_1' = \frac{n\sin\theta\left(\dfrac{m_1 - a}{\cos\theta} - n(t+\pi)\sin\theta\right)}{i_{12}^2\sqrt{m_1^2 + n^2}\sqrt{\left[\dfrac{1}{i_{12}}\left(\dfrac{m_1 - a}{\cos\theta} - n(t+\pi)\sin\theta\right)\right]^2 + n^2}}, \quad (18)$$

$$\sigma_2' = -\frac{n\sin\theta\sqrt{m_1^2 + n^2}\left[\dfrac{m_1 - a}{\cos\theta} - n(t+\pi)\sin\theta\right]}{i_{12}^2\left\{\left[\dfrac{1}{i_{12}}\left(\dfrac{m_1 - a}{\cos\theta} - n(t+\pi)\sin\theta\right)\right]^2 + n^2\right\}^{3/2}}. \quad (19)$$

$n > 0$ is supposed in section 1.3. The meshing radius of the driven contact curves should be above zero (see Eq. 30 in Section 2.2), so:

$$\frac{m_1 - a}{\cos\theta} - n(t+\pi)\sin\theta > 0. \qquad (20)$$

If $\theta \neq 0$ and $\theta \neq \pi$ are supposed, then:

$$\sin\theta > 0, \qquad (21)$$

$$\left\{\left[\frac{1}{i_{12}}\left(\frac{m_1 - a}{\cos\theta} - n(t+\pi)\sin\theta\right)\right]^2 + n^2\right\}^{3/2} > 0, \quad (22)$$

$$i_{12}^2 > 0, \qquad (23)$$

$$\sqrt{m_1^2 + n^2} > 0. \qquad (24)$$

From Eqs. (20) to (24), it can be concluded that $\sigma_1' > 0$ and $\sigma_2' < 0$. Therefore, in the non-vertical HCMWs, $\sigma_1$ is monotonically increasing while $\sigma_2$ is monotonically decreasing.

The same monotonicity can be attained in the vertical HCMWs. The only difference is that the meshing radius of the driven contact curves (see Eq. 30 in section 2.2) is required as:

$$-(nt + n\pi - b) > 0. \qquad (25)$$

From Eqs. (20) and (25), the maximum limit of $t$ is denoted as $t_{max}$ uniformly:

$$t_{max} = \begin{cases} \dfrac{m_1 - a}{n\cos\theta\sin\theta} - \pi & (\theta \neq \pi/2) \\[2mm] \dfrac{b}{n} - \pi & (\theta = \pi/2) \end{cases}. \qquad (26)$$

As shown in Fig. 3, $\sigma_1' \to 0$ and $\sigma_2' \to 0$ if $t \to t_{max}$. Therefore, from Eqs. (14) to (17) and (26), the maximum $\sigma_1$ and the minimum $\sigma_2$ are as in Eqs. (27) and (28) for both non-vertical and vertical cases:

$$\sigma_1 \to \sigma_{1max} = 1 - \frac{n}{\sqrt{m_1^2 + n^2}}, \qquad (27)$$

$$\sigma_2 \to \sigma_{2min} = 1 - \frac{\sqrt{m_1^2 + n^2}}{n}. \qquad (28)$$
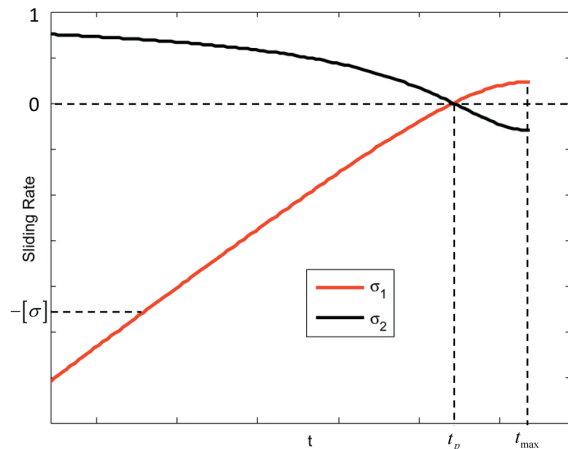


**Fig. 3.** *Monotonicity and feasible region of sliding rate equations*

It should be noted that $\theta \neq 0$ and $\theta \neq \pi$ are supposed in Eqs. (21) and (22). The non-vertical HCMWs when $\theta = 0$ or $\theta = \pi$ are also called parallel-axis HCMWs. Their driving and driven contact curves are circular helix curves, and their slide rates equations are constant functions. However, the maximum values of $\sigma_1$ and $\sigma_2$ are the same as Eqs. (27) and (28).

The allowable slide rate is denoted as $[\sigma]$, $[\sigma] > 0$. According the monotonicity of $\sigma_1$ and $\sigma_2$, their feasible regions are shown in Fig. 3 and Table 1. In Fig. 3, the intersection of the two curves is defined as a pitch

position, i.e. $t = t_p$. It can be concluded that if and only if $t = t_p$,

$$\sigma_1 = \sigma_2 = 0 \qquad (29)$$

In the following section, Eq. (29) will be used to obtain the optimal meshing condition of the HCMW.

**Table 1.** *Feasible region of sliding Rates*

|  | $t < t_p$ | $t = t_p$ | $t_p < t < t_{max}$ |
|---|---|---|---|
| $\sigma_1$ | $0 < |\sigma_1| < [\sigma]$ | 0 | $0 < \sigma_1 < 1$ |
| $\sigma_2$ | $0 < \sigma_2 < 1$ |  | $0 < |\sigma_2| < [\sigma]$ |

## 2.2 Optimal Meshing Condition of the HCMW and Position-Parameter Selection Criterion

The driven contact curve is either a common conical helical curve in a non-vertical case or a planar Archimedean helix in a vertical case. Therefore, from Eqs. (9) and (10), the helical radius of the driven contact curve is defined as Eq. (30):

$$m_2 = \begin{cases} \dfrac{m_1 - a}{\cos\theta} - n(t+\pi)\sin\theta & (\theta \neq \pi/2) \\ -(nt + n\pi - b) & (\theta = \pi/2) \end{cases}. \qquad (30)$$

When $t = t_p$, $m_2 = m_{2p}$ is defined as pitch radius of the driven contact curve. From Eqs. (29) and (30), it can be derived that when $t = t_p$,

$$m_{2p} = i_{12} m_1. \qquad (31)$$

Eq. (31) is defined as the optimal meshing condition of the HCMW. From Eq. (30), the range of $m_2$ depends on the value range of $t$ and thus the range of $m_2$ may not cover $m_{P2}$. To guarantee that the entire meshing process has appropriate average slide rates, it is recommended that:

$$t_p = (t_S + t_E)/2. \qquad (32)$$

From Eqs. (30) to (32), the position-parameter for the non-vertical HCMW case is:

$$a = (1 - i_{12}\cos\theta)m_1 - n\sin\theta\cos\theta\big((t_S + t_E)/2 + \pi\big), (33)$$

and for the vertical HCMW is:

$$b = i_{12}m_1 + n\big((t_S + t_E)/2 + \pi\big). \qquad (34)$$

Eqs. (33) and (34) can serve as the selection criterion of the position-parameters for the HCWM.

Substituting Eq. (33) into Eq. (9), or substituting Eq. (34) into Eq. (10), the same equations of the driven contact curve can be attained:

$$\begin{cases} x_M^{(2)} = \big(i_{12}m_1 + n\sin\theta\big((t_S + t_E)/2 - t\big)\big)\cos\dfrac{t+\pi}{i_{12}} \\ y_M^{(2)} = -\big(i_{12}m_1 + n\sin\theta\big((t_S + t_E)/2 - t\big)\big)\sin\dfrac{t+\pi}{i_{12}} \\ z_M^{(2)} = -n(t+\pi)\cos\theta \end{cases}$$

$$(0 \leq \theta \leq \pi). \qquad (35)$$

## 3 DESIGN EXAMPLE

In this section, the HCMW with different position-parameters are designed as examples both in simulation and a practical experiment to verify their transmission continuity; their slide rates will also be calculated for comparison.

### 3.1 Contact Curve Equations

For the design of the HCMW, $\theta$ is determined according to the directions of the input and out shafts; $i_{12}$ according to the transmission demand; $m_1$, $n$ and the driving and driven tine radii, which are denoted as $r_1$ and $r_2$, according to the bear capable demand [14]; $t_s$ and $t_E$, i.e. the range of $t$, according to the contact curve lengths desired.

With the parameters given above, the driving and driven contact curves can be derived from Eqs. (8) and (35). The corresponding position-parameter for installation, either $a$ or $b$, can be derived with Eq. (33) or Eq. (34).

**Table 2.** *Parameters chosen*

| $\theta$ | $i_{12}$ | $m_1$ | $n$ | $t_s$ | $t_E$ | $Z_1$ | $Z_2$ | $r_1$ | $r_2$ |
|---|---|---|---|---|---|---|---|---|---|
| $2\pi/3$ | 2 | 6 mm | 6 mm | $-\pi$ | $-\pi/2$ | 6 | 12 | 0.6 mm | 0.5 mm |

To be more specific, numerical examples of non-vertical HCMWs are provided, and the parameters are chosen as in Table 2.

From Table 2, the contact ratio $\xi = Z_1(t_E - t_s)/2\pi = 1.25$ [13]. From Table 2 and Eqs. (8) and (35), the driving and driven contact curves are as below:

$$\begin{cases} x_M^{(1)} = 6\cos t \\ y_M^{(1)} = 6\sin t \\ z_M^{(1)} = 6(\pi + t) \end{cases}, \qquad (36)$$

$$\begin{cases} x_M^{(2)} = \left(12 - 3\sqrt{3}\left(t + 3\pi/4\right)\right)\cos\dfrac{t+\pi}{2} \\ y_M^{(2)} = -\left(12 - 3\sqrt{3}\left(t + 3\pi/4\right)\right)\sin\dfrac{t+\pi}{2}. \qquad (37) \\ z_M^{(2)} = 3\left(t + \pi\right) \end{cases}$$

From Eq. (31), $m_{2p} = 12$ mm and from Eq. (33), $a_p = 14.041$ mm.

As a comparison, with the same driving contact curve, the previous driven contact curve [9] is derived from Eq. (9) as below:

$$\begin{cases} x_M^{(2)} = \left(2a - 12 - 3\sqrt{3}\left(t + \pi\right)\right)\cos\dfrac{t+\pi}{2} \\ y_M^{(2)} = -\left(2a - 12 - 3\sqrt{3}\left(t + \pi\right)\right)\sin\dfrac{t+\pi}{2}. \qquad (38) \\ z_M^{(2)} = 3\left(t + \pi\right) \end{cases}$$

From Eq. (20), $a > 10.081$ mm is required. Different values of $a$ are selected as Table 3. An equation of the driven contact curve can be derived by submitting each value of $a$ into Eq. (38). It is worth noticing that Eq. (37) is equal to Eq. (38) when $a_3 = 14.041$ mm.

**Table 3.** Values of $a$ [mm]

| $a_1$ | $a_2$ | $a_3$ $(a_p)$ | $a_4$ | $a_5$ |
|---|---|---|---|---|
| 12.041 | 13.041 | 14.041 | 15.041 | 16.041 |

### 3.2 Simulation

As shown in Fig. 4, according to the parameters in Table 2 and the different $a$ values in Table 3, a driving wheel and driven wheels of different sizes can be attained in Pro/Engineering.
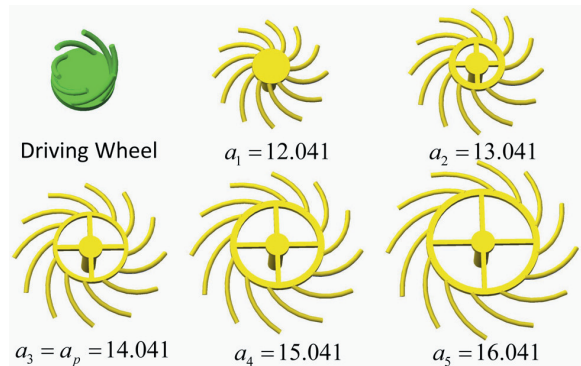


**Fig. 4.** *Simulation of driving and driven wheels*

As shown in Fig. 5, these driven wheels can mesh with the same driving wheel. It can be concluded that the value of $a$ influences the intersection point of the center lines of driving and driven wheels. The values of $a$ mainly change the meshing radii of the driven wheels and subsequently the slide rates of the HCMW pairs.
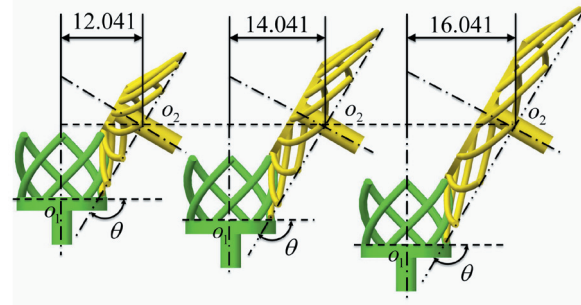


**Fig. 5.** *Different driven wheels meshing with the same driving wheels*

### 3.3 Transmission Continuity Test

As shown in Fig. 6, the driving wheel and the driven wheels were manufactured through selective laser melting (SLM) technology [16] and post-processed with electrochemical brushing process [15]. Within the processing capacity of the SLM, the manufacturing cost decreases as the weight of the HCMW decreases. Mainly operating in conditions with low loads, the HCMW is usually small and light. Therefore, the SLM technology was chosen in this paper and will be recommended for large-scale industry.

To verify their transmission continuity, the rotation speeds of the wheels were measured with a test rig developed by our research team [9], which is shown in Fig. 7. The test procedure is shown in Fig. 8, and the test condition in Table 4.



**Fig. 6.** *Manufactured driving wheel and driven wheels*
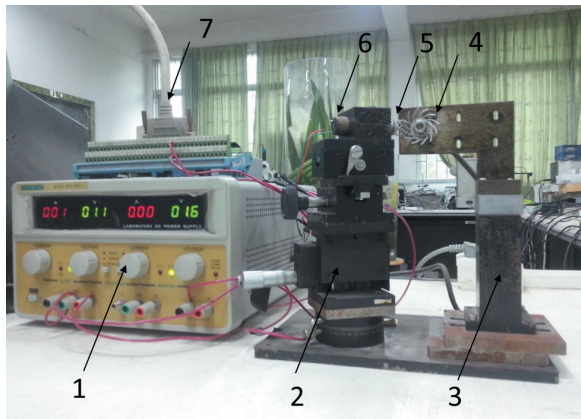
**Fig. 7.** *Test rig: 1) DC power, 2) 4-DOF moveable platform, 3) fixed bracket, 4) driven wheel, 5) driving wheel, 6) DC motor, and 7) cable connected to acquisition card and computer*

**Table 4.** *Test condition*

| | |
|---|---|
| Voltage on motor | 1.1 V |
| Currency on motor | 0.1 A |
| Angular velocity of motor shaft | 36° / s |
| Torque transmitted | 0.18 Nm |
| Encoder Data-acquisition frequency | 1 Hz |
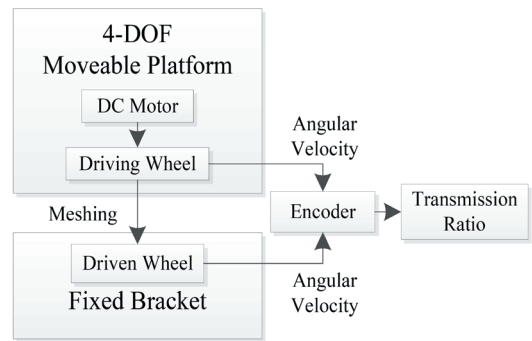


**Fig. 8.** *Test procedure*

**Table 5.** *Transmission ratio*

| $a$ | $a_1$ | $a_2$ | $a_3$ | $a_4$ | $a_5$ |
|---|---|---|---|---|---|
| Practical value | 1.99 | 2.00 | 2.00 | 2.01 | 2.00 |
| Theoretical value | | | 2 | | |
| Relative error [%] | 0.5 | 0 | 0 | 0.5 | 0 |

Continuous records of the test are shown in Fig. 9. As shown in Table 5, all the driven wheels can continuously commit the transmission within the allowable error range [9].
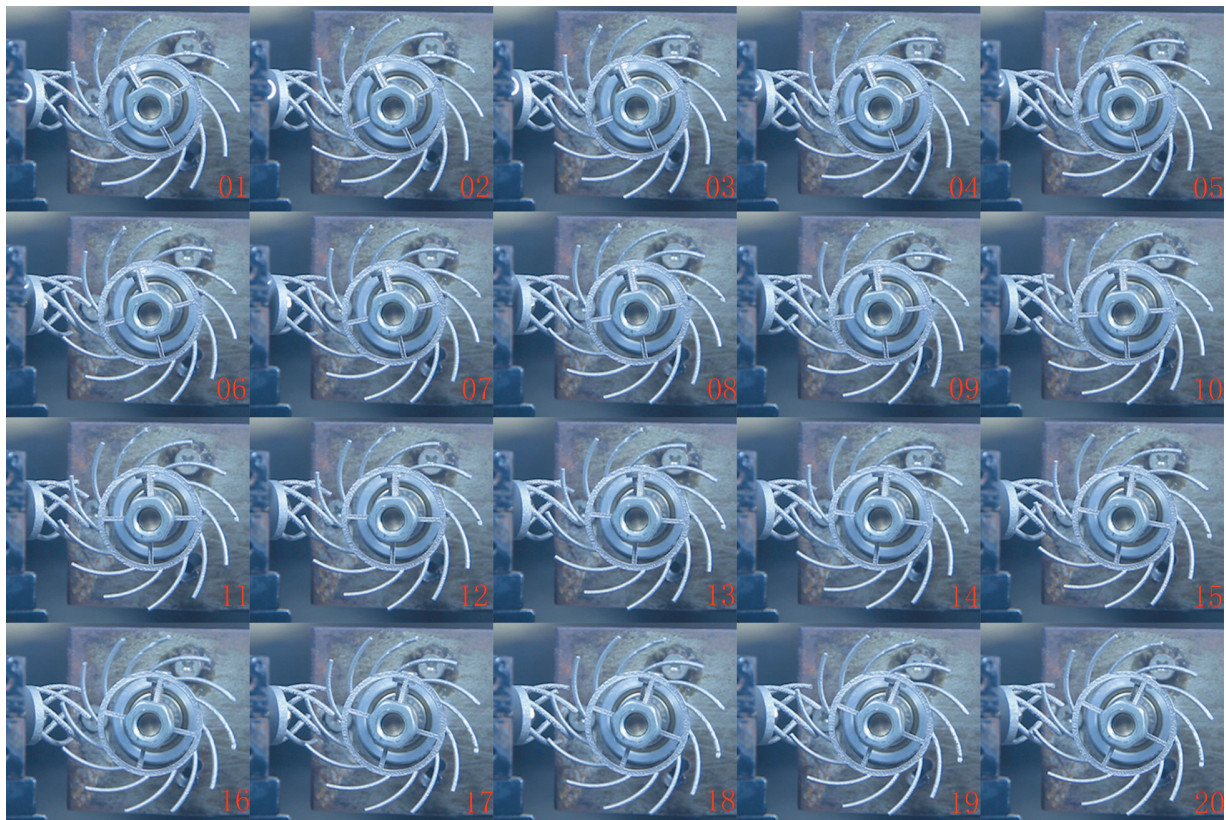


**Fig. 9.** *Continuous records of the test*

**Table 6.** *Maximum absolute values of $\sigma_1$ and $\sigma_2$ corresponding to different $a$*

| $a$ [mm] | 12.041 | 13.041 | 14.041 | 15.041 | 16.041 |
|---|---|---|---|---|---|
| Range of $\sigma_1$ | −0.003 to 0.249 | −0.090 to 0.202 | −0.182 to 0.141 | −0.279 to 0.069 | −0.379 to −0.012 |
| $|\sigma_1|_{max}$ | 0.249 | 0.202 | 0.182 | 0.279 | 0.379 |
| Range of $\sigma_2$ | 0.012 to 0.275 | −0.074 to 0.218 | −0.164 to 0.154 | −0.253 to 0.083 | −0.332 to 0.003 |
| $|\sigma_2|_{max}$ | 0.275 | 0.218 | 0.164 | 0.253 | 0.332 |
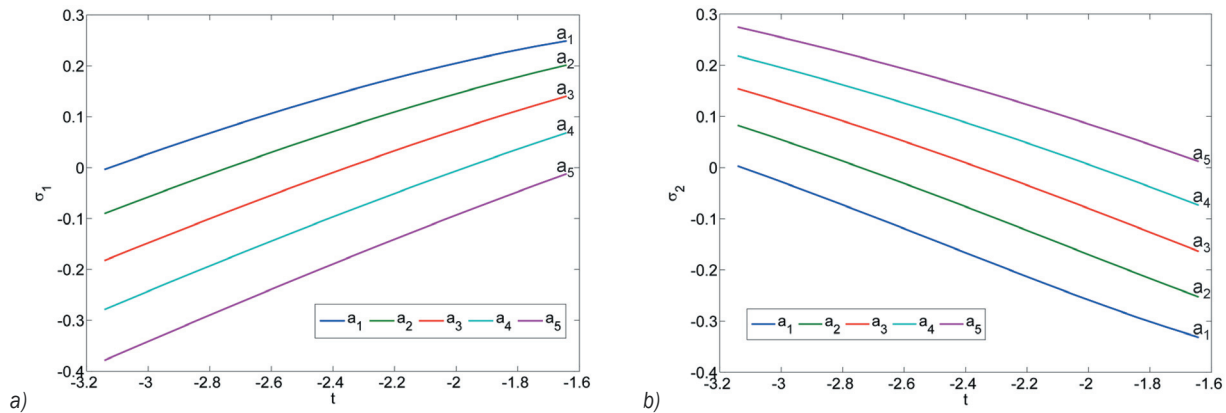


**Fig. 10.** *Slide rates of the driving and driven contact curves; a) $\sigma_1$ vs. t and b) $\sigma_2$ vs. t*

It should be noted that the accuracy of setting the parameter $a$ in the test rig is 0.1 mm, which is much lower the accuracy of the simulation in the previous section and the theoretical calculation in the next section. Furthermore, only the transmission continuity of the HCMWs is verified in the experiment.

### 3.4 Slide Rate Discussion

As shown in Fig. 10, the slide rates of Eq. (38) with different position-parameters are calculated from Eqs. (14) and (15) and drawn with MATLAB.

As shown in Table 6, the ranges of $\sigma_1$ and $\sigma_2$ are measured from Fig. 9. Since the signs of $\sigma_1$ and $\sigma_2$ indicate the relative slide direction, only the maximums of their absolute values are compared. The result shows that when $a = a_p = 14.041$ mm, both $|\sigma_1|_{max}$ and $|\sigma_2|_{max}$ achieve their minimums simultaneously. Although all five pairs of the HCMW can mediate the transmission, the one coincident with the position-parameter selection criterion has the best slide rates.

### 4 CONCLUSIONS AND PROSPECTS

This paper presents the position-parameter selection criterion of the HCMW based on its slide rates. Specifically, the results can be concluded as below:

1. The optimal meshing condition is attained from the analysis of the slide rate, and it shows that the slide rates of the HCMW are zero if and only if the meshing radius of the driven contact curve equals the product of the transmission ratio and the meshing radius of the driving contact curve;
2. The mesh at the midpoint of the contact curves should be coincident with optimal meshing condition, which is defined as the position-parameter selection criterion;
3. Numerical examples show that the HCMWs coincident with the position-parameter selection criterion that possesses the best slide rates.

However, some issues remain to be improved: an experimental measure method of the HCMW slide rates has yet to be proposed; the slide rates' effects on the friction and wear of the HCMW remain to be explored; the forming conditions of the hydrodynamic film should be studied to determine whether the HCMW will work with lubricant in the future; furthermore, the allowable slide rates under lubricant condition need to be determined for standardization production.

### 5 ACKNOWLEDGMENT

## 6 NOMENCLATURE

$a$    Position-parameter, distance from point $o_p$ to axis $z$

$b$    Position-parameter, distance from point $o_p$ to axis $x$

$i_{12}$    Transmission ratio

$M$    Meshing point

$\widehat{MM_1}$    Arc length between $M$ and $M_1$

$\widehat{MM_2}$    Arc length between $M$ and $M_2$

$\overline{MM_1}$    Contact vector from $M$ and $M_1$

$\overline{MM_2}$    Contact vector from $M$ and $M_2$

$n$    Pitch parameter of driving curve

$\boldsymbol{r}_1$    Driving curve equation in vector form

$r_1$    Driving tine radius

$\boldsymbol{r}_2$    Driven curve equation in vector form

$r_2$    Driven tine radius

$s_1$    Arc length on driving curve

$s_2$    Arc length on driven curve

$t$    Scope parameter of helix curve

$t_s$    Starting value of $t$

$t_E$    Ending value of $t$

$t_p$    $t$ when HCMW in pitch position

$t_{max}$    Maximum available value of $t$

$Z_1$    Number of driving tines

$Z_2$    Number of driven tines

$\Gamma_1$    Driving curve

$\Gamma_2$    Driven curve

$\theta$    Included angle between angular velocity vectors

$\sigma_1$    Slide rate of driving curves

$\sigma_2$    Slide rate of driven curves

$[\sigma]$    Available slide rate

(superscript)    Corresponding coordinate

## 7 REFERENCES

[1] Wu, X.T. (2009). *Principle of Gearing*. Xi'an Jiaotong University Press, Xi'an. (in Chinese)

[2] Litvin, F.L. (2008). *Gear Geometry and Applied Theory*. Shanghai Science and Technology Publishers, Shanghai. (in Chinese)

[3] Bergseth, E. Björklund, S. (2010). Logarithmical crowning for spur gears. *Strojniški vestnik - Journal of Mechanical Engineering*, vol. 56, no. 4, p. 239-244.

[4] Staniek, R. (2011). Shaping of face toothing in flat spiroid gears. *Strojniški vestnik - Journal of Mechanical Engineering*, vol. 57, no. 1, p. 47-54, DOI:10.5545/sv-jme.2010.093.

[5] Puccio, F.D., Gabiccini, M., Guiggiani, M. (2006). Generation and curvature analysis of conjugate surfaces via a new approach. *Mechanism and Machine Theory*, vol. 41, no. 4, p. 382-404, DOI:10.1016/j.mechmachtheory.2005.07.008.

[6] Ciulli, E., Bartilotta, I., Polacco, A., Manconi, S., Vela, D. (2010). A model for scuffing prediction. *Strojniški vestnik - Journal of Mechanical Engineering*, vol. 54, no. 4, p. 267-274.

[7] Chen, Y.Z., Xing, G.Q., Peng, X.F. (2007). The space curve mesh equation and its kinematics experiment. *12th IFToMM World Congress*, Besançon.

[8] Chen, Y.Z., Xiang X.Y., Luo, L. (2009). A corrected equation of space curve meshing. *Mechanism and Machine Theory*, vol. 44, no. 7, p. 1348-1359, DOI:10.1016/j.mechmachtheory.2008.11.001.

[9] Ding, J., Chen, Y.Z., Lv, Y.L. (2012). Design of Space-Curve Meshing-Wheels with Unequal Tine Radii. *Strojniški vestnik - Journal of Mechanical Engineering*, vol. 58, no. 11, p. 633-641, DOI:10.5545/sv-jme.2012.493.

[10] Chen, Z., Chen, Y.Z., Ding, J. (2013). A generalized space curve meshing equation for arbitrary intersecting gear. *Proceedings of the Institution of Mechanical Engineers, Part C: Journal of Mechanical Engineering Science*, vol. 227, no. 7, p. 1599-1607, DOI:10.1177/0954406212463310.

[11] Chen, Y.Z., Lv, Y.L., Ding, J, Chen, Z. (2013). Fundamental design equations for space curve meshing skew gear mechanism. *Mechanism and Machine Theory*, vol. 70, p. 175-188, DOI:10.1016/j.mechmachtheory.2013.07.004.

[12] Chen, Y.Z., Hu, Q., Su, L. (2010). Design criterion for the space-curve meshing-wheel transmission mechanism based on the deformation of tines. *Journal of Mechanical Design*, vol. 132, no. 5, p. 054502, DOI:10.1115/1.4001535.

[13] Chen, Y.Z., Luo, L., Hu, Q. (2009). The contact ratio of a space-curve meshing-wheel. *Journal of Mechanical Design*, vol. 131, no.7, p. 074501, DOI:10.1115/1.3116343.

[14] Liang, S.K., Chen, Y.Z. (2012). Research on the maximum bending stress on driving tine of SCMW. *Applied Mechanics and Materials*, vol. 184-185, p. 445-449, DOI:10.4028/www.scientific.net/AMM.184-185.445.

[15] Chen, Y.Z., He, E.Y., Chen, Z. (2012). Investigations on precision finishing of space curve meshing wheel by electrochemical brushing process. *The International Journal of Advanced Manufacturing Technology*, vol. 67, no. 9-12, p. 2387-2394, DOI:10.1007/s00170-012-4659-1.

[16] Chen, Y.Z., Sun, L.H, Wang, D., Yang, Y.Q., Ding, J. (2010). Investigation into the process of selective laser melting rapid prototyping manufacturing for space-curve-meshing-wheel. *Advanced Material Research*, vol. 135, p. 122-127, DOI:10.4028/www.scientific.net/AMR.135.122.

[17] Chen, Y.Z., Chen, Z., Ding, J. (2011). *Space Curve Mesh Driving Pair and Polyhedral Space Curve Mesh Transmission*, US Patent, Aplication no. PCT/

CN2010/078294, US Patent and trademark office, Washington D.C.

[18] Chen, Y.Z., Fu, X.Y., Ding, J., Liang, S.K. (2013). Geometric Design of Micro-Reducer With Multi-Output Shafts Distributed in Regular Polygon Form. *Journal of Mechanical Design*, vol. 135, no. 5, p. 051104, DOI:10.1115/1.4024084.

[19] Chen, Y.Z., Ding, J., Yao, C.H., Lv, Y.L. (2012). Polyhedral space curve meshing reducer with multiple output shafts. *ASME 2012 International Mechanical Engineering Congress & Exposition*, Houston, vol. 3, p. 1505-1511, DOI:10.1115/IMECE2012-86087.

[20] Chen, Y.Z., Chen, Z, Ding, J. (2013). *Space Curve Mesh Driving Pair and Polyhedral Space Curve Mesh Transmission,* U.S. Patent, Appliacion No. 20130145876, US Patent and trademark office, Washington D.C.

[21] Chen, Y.Z., Ding, J., Lv, Y. (2013) Design of polyhedral helix curve meshing reducer. *Journal of Mechanical Design*, vol. 136, no. 4, paper no. 044503, DOI:10.1115/1.4026571.